Available online at www.sciencedirect.com
ScienceDirect
Trans. Nonferrous Met. Soc. China 24(2014) 3840−3847
Transactions of Nonferrous Metals Society of China
www.tnmsc.cn

Isothermal annealing of cold-rolled Al−Mn−Fe−Si alloy with different microchemistry states

Ke HUANG[1], Yan-jun LI[1,2], Knut MARTHINSEN[1]

1. Department of Materials Science and Engineering, Norwegian University of Science and Technology, Trondheim 7491, Norway;
2. SINTEF Materials and Chemistry, Trondheim 7465, Norway

Received 17 October 2013; accepted 23 October 2014

Abstract: Microstructural evolution of a cold-rolled Al−Mn−Fe−Si alloy during annealing was studied. Except the as-cast variant, two other different homogenizations were considered, one gave a high density of fine dispersiods providing a considerable Zener drag influencing the softening behavior while the other gave a lower density of coarser dispersoid structure providing a much smaller drag effect. The gradual microstructural evolutions during annealing for the three variants were captured by interrupting annealing at different time. Effects of microchemistry state on recrystallization kinetics, recrystallized grain structure and texture were characterized by EBSD. It is demonstrated that the actual softening kinetics, final microstructure and texture are a result of delicate balance between processing condition and microchemistry state. Strong concurrent precipitation takes place in the case with high concentration of Mn in solid solution, which suppresses nucleation and retards recrystallization and finally leads to grain structure of coarse elongated grains dominated by a P texture component together with a ND-rotated cube component. On the contrary, when solute content of Mn is low and pre-existing dispersoids are relatively coarser, faster recrystallization kinetics is exhibited together with an equiaxed grain structure with mainly cube texture.

Key words: aluminum alloy; Al−Mn−Fe−Si alloy; recrystallization kinetics; microchemistry; precipitation; recrystallization texture

1 Introduction

It is well established that particles are of the outmost importance in recrystallization of alloys containing second-phase particles [1−6]. Small and numerous dispersoids (typically formed during homogenization and/or subsequent heat treatments) tend to hinder boundary motion and slow down recrystallization and grain growth through a Zener drag effect [7]. With a sufficiently small spacing of thermally stable particles, it is even possible to preserve the deformed/recovered microstructure up to the melting temperature of the matrix [8]. By contrast, widely spaced coarse constituent particles larger than ~1 μm, formed during casting, can accelerate recrystallization by particle stimulated nucleation (PSN) due to the large amount of stored energy that concentrates next to them during cold rolling [9]. It is well documented that a suitable homogenization cycle may strongly facilitate the down-stream recrystallization of Al sheet by providing different microchemistry states (solid solution levels, constituent particles and dispersoids) [10−18]. However, the effects and mechanisms behind are neither well understood nor quantitatively described. The objective of the present work was to investigate the effect of microchemistry introduced by homogenization on the softening behavior of a cold-rolled Al−Mn−Fe−Si alloy. The effects of microchemistry state on the fully recrystallized grain structure and texture have been investigated and presented elsewhere [19]. The focus of the present work is on identifying the effect of pre-existing dispersoids and concurrent precipitation on the nucleation and subsequent microstructural evolution during isothermal annealing. It is part of a comprehensive investigation on particle-annealing interactions in AA3xxx alloys involving both industrial and academic partners, being the objective to obtain a better understanding of the evolution of microstructure and texture and their interactions with second-phase particles during cold rolling and subsequent annealing of AA 3xxx type alloys [19−24], as basis for validation and further development of relevant microstructure models [25,26] accounting for these aspects.

Corresponding author: Ke HUANG; Tel: +47-73594004; E-mail: ke.huang@ntnu.no; huangke0729@hotmail.com
DOI: 10.1016/S1003-6326(14)63541-X

2 Experimental

2.1 Alloy conditions and annealing treatment

The investigated alloy was received from hydro aluminium as a DC-cast AA3xxx extrusion billet. The as-received material, denoted as C1, was in the as-cast state, with the chemical composition of 0.4% Mn, 0.5% Fe, 0.15% Si. The material possessed grains of equiaxed shape with an average size of ~140 μm, and more details can be found elsewhere [19−21].

The as-received C1 material was subsequently homogenized at two different conditions to get different microchemistry, i.e. amount of solute (mainly Mn) and second-phase particle. The homogenization treatments were performed in an air circulation furnace with a temperature accuracy of ±2 K, starting from room temperature (about 20 °C). One set of the samples for C1 was heated at 50 °C/h to 450 °C and kept for 4 h, referred to as C1-2. Another set of the samples was subjected to a two-stage homogenization treatment. First, the samples were heated at 50 °C/h to 600 °C and held at this temperature for 4 h, then the samples were cooled at 25 °C/h to 500 °C and kept for another 4 h, which gives the C1-3 homogenized condition. The as-cast material was designated as C1-0. Materials were water-quenched to room temperature at the end of the homogenization procedure to freeze the state of supersaturation/ precipitation potential.

The homogenized materials together with the materials of the as-cast condition, were cold-rolled to deformation strain ε of 1.6. The rolled sheets were subsequently isothermally back-annealed in a pre-heated salt bath at prescribed temperatures with different holding time in the range of $5-10^5$ s, followed by quick water quenching.

2.2 Microstructure characterization

The softening and precipitation behaviors during annealing were followed by Vickers hardness (HV) and electrical conductivity (EC) measurements performed on the RD−TD plane of sheets. Each reported value was obtained by averaging eight measurements. Electrical conductivity was measured by a Sigmascope EX 8 instrument at room temperature of about 293 K (20 °C). It has been observed elsewhere that the concentrations of Fe and Si in solid solution of similar alloy are very small and vary little during heat treatment, so it is reasonable to assume that the evolution of EC is mainly due to the variation of Mn in solid solution [27]. Thus, it can be used as a semi-quantitative measure of the concurrent precipitation of Mn-containing particles. Metallographic examinations of constituent particles and dispersoids were carried out by backscattered electron channeling contrast imaging on a Zeiss Ultra 55 field emission gun scanning electron microscope (FEG-SEM). Images were captured electronically and analyzed with standard image analysis software. Characteristic size parameters of constituent particles, equivalent diameter (d) and number density were measured with the image analysis software Image-J. For the hardness measurements, a load of 1 kg, a loading time of 15 s and a loading speed of 100 μm/s were used.

The crystallographic textures of the sheets were measured by means of EBSD (electron backscattered diffraction), the same Zeiss Supra/Ultra 55 scanning electron microscope (SEM) as mentioned above, and TSL software. Orientation maps of both deformed and annealed samples, covering typically more than 1000 grains (except the cases with extremely large grains), with step size of 1−2 μm, were used to study the orientation of the recrystallized grains and thus the texture evolution during recrystallization.

Selected conditions were characterized by SEM/ EBSD so that the effect of homogenization and level of Mn in solid solution on the softening behavior in terms of microstructure and texture evolution the different homogenized conditions could be studied. For all of the micrographs presented in this work, the horizontal direction corresponds to rolling direction (RD) while the vertical direction is the normal direction (ND). The grain size was measured as the equivalent diameter in the RD−ND cross section. The texture was represented in terms of orientation distribution functions (ODFs) using TSL OIM Analysis 6 software package by imposing orthotropic (rolling) sample symmetry, and using the harmonic series expansion method (L=22) with a Gaussian half-width of 5° [28].

3 Results and discussion

3.1 Microchemistry state before annealing

The micrographs of the particle distribution for the three variants (before deformation) are presented elsewhere [19]. From this work, it is clear that the variant homogenized at the lower temperatures, i.e. C1-2, obviously has more but finer dispersoids than its counterpart C1-3, as illustrated in Table 1. It is important to note that the dispersoids are shown to have a more or less even spatial distribution [19]. The constituent particles increase slightly in size for C1-2 as compared with C1-0. When homogenized at higher temperatures (C1-3), constituent particles were observed to grow to 1.10 μm.

3.2 Effect of microchemistry state on evolution of microstructure and texture

The annealing behaviors of the samples cold-rolled

Table 1 Electrical conductivity, concentrations of solutes, diameter and number density of particles [19]

Sample	Electrical conductivity/ ($MS \cdot m^{-1}$)	w(Mn)/%	Constituent particle		Dispersoid	
			Diameter/μm	Number density/mm^2	Diameter/μm	Number density/mm^2
C1-0	23.9	0.35	0.88	2.8×10^4	–	–
C1-2	27.5	0.16	0.96	2.9×10^4	0.054	1.3×10^6
C1-3	29.0	0.11	1.10	2.1×10^4	0.127	5.5×10^4

to ε=1.6 in terms of hardness and electrical conductivity evolution during annealing at 400 °C are shown in Fig. 1. Recrystallization kinetics becomes faster when the content of Mn in solid solution prior to annealing decreases from C1-0 to C1-3 (see Fig. 1(a)). This is accompanied by a decreasing amount of concurrent precipitation from C1-0 to C1-3, as indicated by the variation of electrical conductivity in Fig. 1(b).

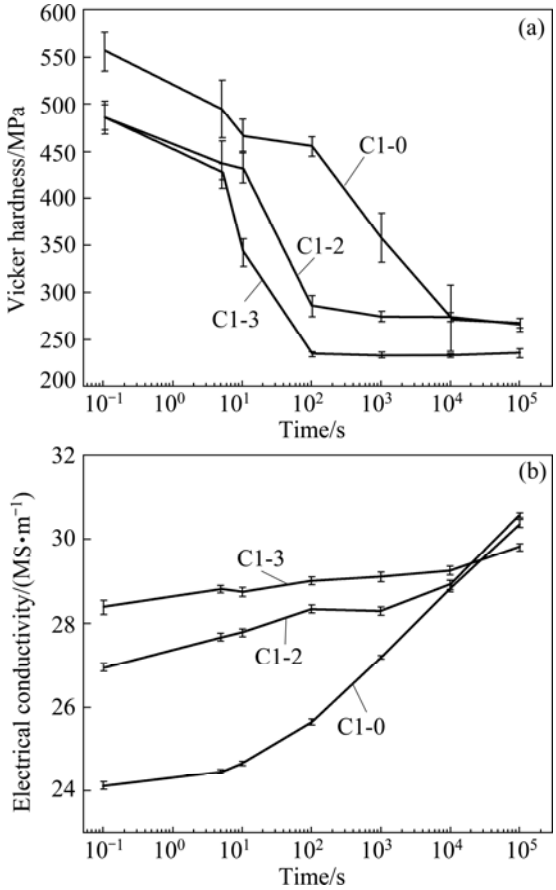

Fig. 1 Variation of hardness (a) and electrical conductivity (b) during annealing at 400 °C for three variants cold-rolled to ε=1.6

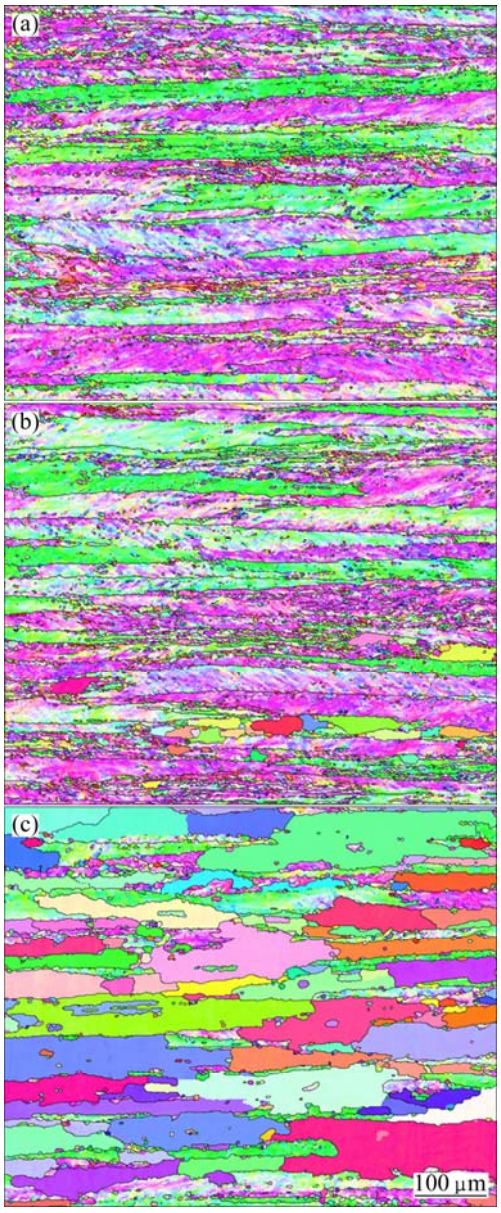

Fig. 2 EBSD maps showing microstructure of three variants during annealing at 400 °C: (a) C1-0, ε=1.6, t=10 s; (b) C1-0, ε=1.6, t=100 s; (c) C1-0, ε=1.6, t=1000 s

The microstructure and texture evolution during annealing of the cold-rolled (ε=1.6) C1-0 samples are shown in Figs. 2 and 3, respectively. As shown in Fig. 2(a), even though there are no pre-existing dispersoids, any indications of recrystallization were not observed in the first 10 s of annealing at 400 °C, suggesting a long incubation time and/or a time dependent nucleation behavior rather than site saturated nucleation. A typical rolling texture was obtained at this annealing stage, as illustrated in Fig. 3(a). After a longer annealing time of 100 s, a limited number of recrystallized grains emerge (see Fig. 2(b)), being parts of a few elongated "icelands" of recrystallized material. As observed these grains are already quite large before any visible nuclei have been created at other part

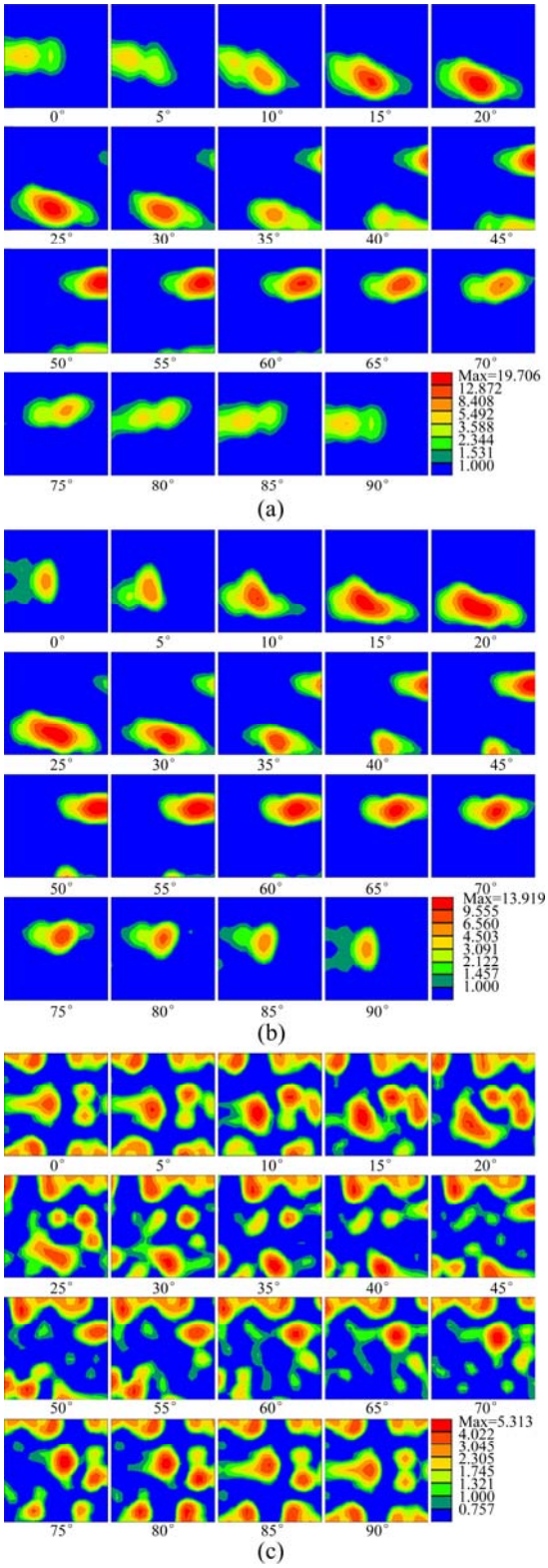

Fig. 3 ODF maps showing texture of three variants during annealing at 400 °C: (a) C1-0, ε=1.6, t=10 s; (b) C1-0, ε=1.6, t=100 s; (c) C1-0, ε=1.6, t=1000 s

of the sample, indicating a heterogeneous nucleation behavior. The strength of the deformation texture components decreases. However, no clear recrystallization texture components show up, most probably since the volume fraction of recrystallized grains is still small (see Fig. 3(b)). These recrystallized grains then continue to grow with further annealing together with nucleation and growth of recrystallized grains at other places (see Fig. 2(c)) in the material. Growth preferentially takes place in the RD direction, indicating that concurrent precipitation, mainly at old (high angle) grain boundaries [30], aligned along the rolling direction, is exerting a dragging force along the ND direction, resulting in the elongated grain shape. A ND rotated cube texture component has shown up, together with indications of P texture (split in two peaks), both components typically observed when concurrent precipitation interacted with recrystallization [29,30]. It should be noted that, after 1000 s annealing, recrystallization is not completed yet and a significant brass texture component is still present.

For the deformed samples of variant C1-2, which has a large number of fine pre-existing dispersoids but lower Mn concentration in solid solution, faster recrystallization was observed when annealing at the same temperature of 400 °C, as can be seen in Fig. 4. Different from variant C1-0 (see Fig. 2(a)), a considerable amount of recrystallized grains are present after annealing for 10 s, and these as-observed grains are slightly elongated along the RD direction (see Fig. 4(a)). This difference must be due to the distinctly different microchemistry states since the thermo-mechanical processing conditions are the same. The faster recrystallization kinetics for the C1-2 sample within the first 10 s indicates that pre-existing dispersoids (i.e. in the form of a Zener drag [8]) have a less profound retarding effect on the recrystallization than concurrent precipitation of Mn-containing dispersoids of a similar amount of Mn. Although the dispersoids resulting from concurrent precipitation are formed at a later stage than the pre-existing ones, and during annealing, their effect on recrystallization is clearly stronger. This observation can be due to several aspects. Firstly, it may be speculated that early precipitation in C1-0 (before onset of recrystallization) gives rise to a high density of very small dispersoids which may provide a higher Zener drag (at this stage) in this alloy than the pre-existing ones in C1-2, more strongly suppressing nucleation than the latter case. Nevertheless, in view of the electrical conductivity evolution, a comparable amount of early precipitation/ removal of Mn from solid solution takes place in C1-2 and C1-0 (see Fig. 1(b)). This fact may indicate that in the former case Mn is primarily consumed by the already existing dispersoids causing mainly coarsening and not new small ones, i.e. actually reducing the Zener drag in this case. Moreover, the initial higher solid solution level of Mn in C1-0 may also act to slow down recovery through a solute drag effect and

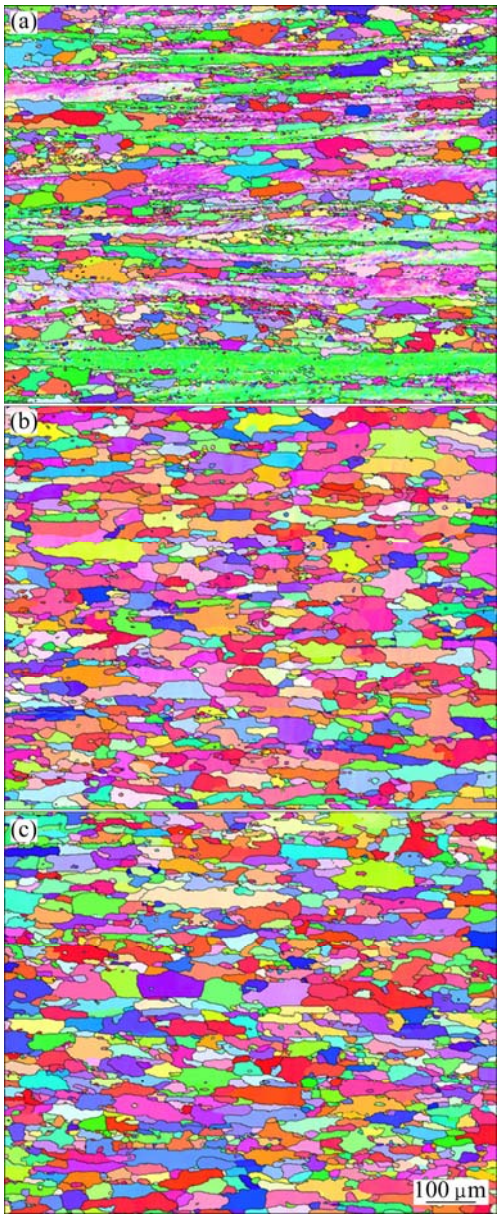

Fig. 4 EBSD maps showing microstructure of three variants during annealing at 400 °C: (a) C1-2, ε=1.6, t=10 s; (b) C1-2, ε=1.6, t=100 s; (c) C1-2, ε=1.6, t=1000 s

thus also suppress/retard nucleation of recrystallization. Secondly, the fact that these two types of dispersoids are differently distributed in the material most probably also plays a role. The pre-existing dispersoids are more randomly distributed [19], while concurrent precipitation mainly occurs at deformed old grain boundaries (along the RD direction) around which nucleation is very active, leading to less nucleation and a directional dragging force.

The texture in this condition (10 s annealing) is still mainly dominated by deformation texture components, although a weak ND-rotated cube component is also visible, as indicated in Fig. 5(a). Recrystallization completed after annealing for 100 s for C1-2 (see Fig. 4(b)). Since mainly more grains and not distinctly larger grains are observed after 100 s of annealing as compared with 10 s, additional nucleation must have taken place, resulting in an average recrystallized size of

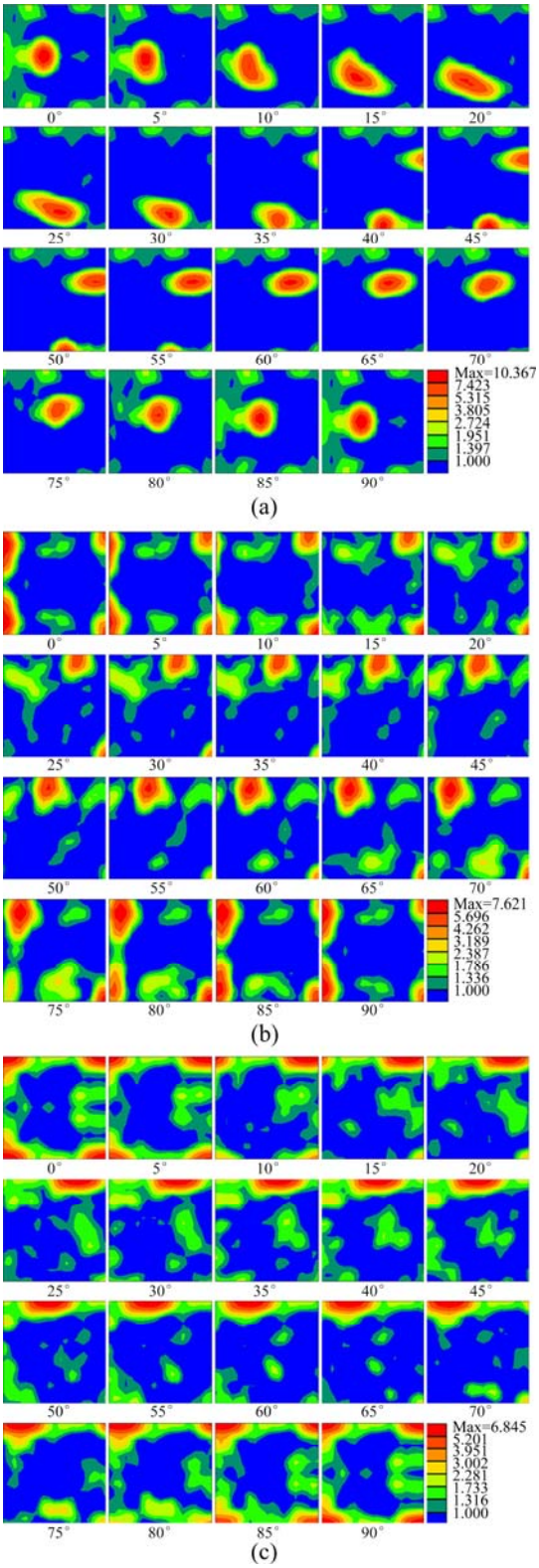

Fig. 5 ODF maps showing texture of three variants during annealing at 400 °C: (a) C1-2, ε=1.6, t=10 s; (b) C1-2, ε=1.6, t=100 s; (c) C1-2, ε=1.6, t=1000 s

~43 μm, much less than that of the recrystallized state of the C1-0 sample. Regarding the texture, the deformation texture is now replaced by a distinct cube texture component (with some TD-rotation), as shown in Fig. 5(b). Further annealing at this temperature does not change the grain shape and size (~43 μm) (see Fig. 4(c)). The evolution of texture is not significant, except that the TD rotation mainly disappears and indications of very weak P component appear (see Fig. 5(c)).

The fastest recrystallization kinetics was observed for the C1-3 sample, as previously shown in Fig. 1(a). It can be ascribed to its limited number of pre-existing dispersoids and the lowest Mn content prior to annealing. Both factors have a negligible contribution to any precipitation−recrystallization interactions. A large number of recrystallized grains were present already after annealing for 10 s, with mainly equiaxed shape, as seen in Fig. 6(a). Still the deformation texture outweighs indications of any recrystallization texture components, e.g., the very weak cube and goss components also present in Fig. 7(a). Annealing to longer time at 400 °C leads to fully recrystallized structures, with an average grain size of ~21 μm, as shown in Figs. 6(b) and (c). The texture of the recrystallized samples is dominated now by the cube component, while typical deformation texture components still exist, even though they diminish along with longer annealing time, as seen in Figs. 7(b) and (c). The texture intensity is in general weaker than that of the C1-2 sample annealed at the same conditions, as well as the recrystallization texture of the same variants after larger deformation [19].

4 Conclusions

1) The microchemistry state has a profound effect on the initial stage of recrystallization. High level of Mn content in solid solution gives significant concurrent precipitation, which suppresses nucleation and only a limited number of recrystallized grains are present with elongated shape due to the exerting dragging force along the ND direction from the concurrent precipitation. A large number of equiaxed grains are nucleated when the concentration level of Mn in solid solution is low, due to less retarding force from the dispersoids.

2) The microchemistry state also affects the recrystallization kinetics. Strong concurrent precipitation strongly suppresses nucleation and retards recrystallization, while the fastest recrystallization is obtained when both the concurrent precipitation and pre-existing dispersoids are less. This indicates that pre-existing dispersoids have less effect on recrystallization than concurrent precipitation during annealing.

3) ND-rotated cube and P components are the dominant texture components when strong concurrent precipitation (relatively high concentration level of Mn prior to annealing) interacts with recrystallization. On the other side, the recrystallization texture is characterized by a distinct cube texture with the same deformation texture components when the interaction between fine dispersoids (pre-existed and concurrently precipitated) and recrystallization is mostly avoided (low content of Mn in solid solution).

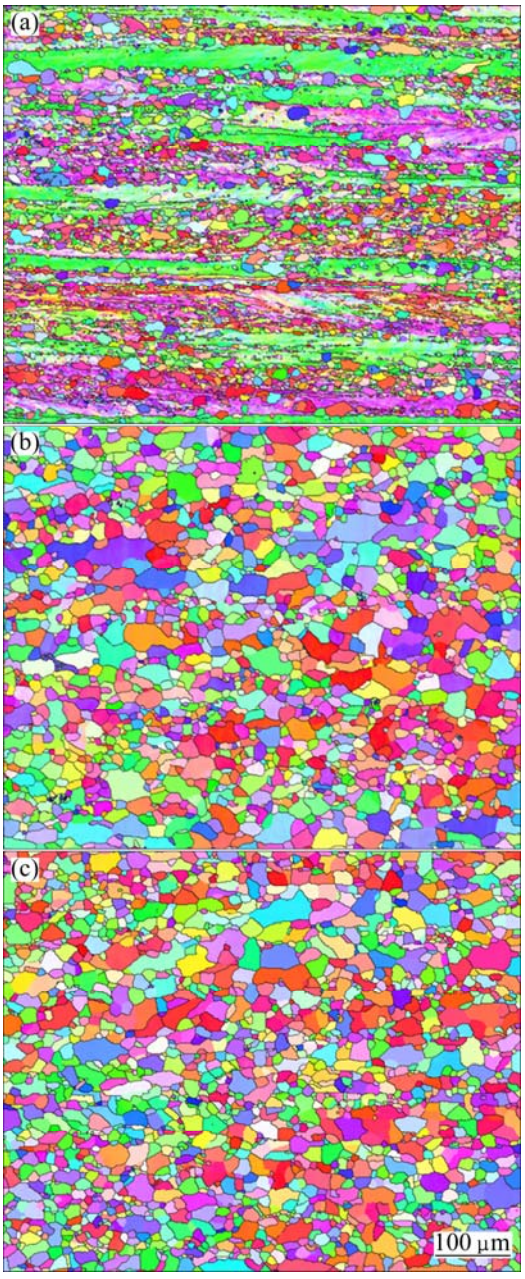

Fig. 6 EBSD maps showing microstructure of three variants during annealing at 400 °C: (a) C1-3, ε=1.6, t=10 s; (b) C1-3, ε=1.6, t=100 s; (c) C1-3, ε=1.6, t=1000 s

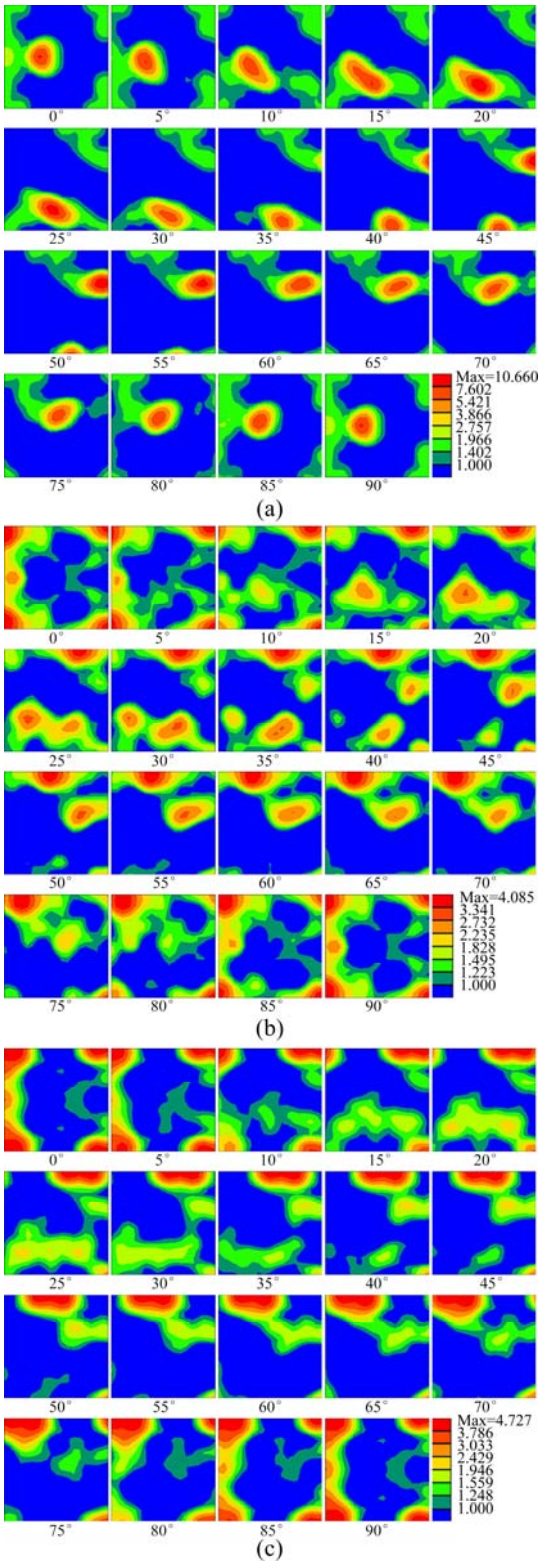

Fig. 7 ODF maps showing texture of three variants during annealing at 400 °C: (a) C1-3, ε=1.6, t=10 s; (b) C1-3, ε=1.6, t=100 s; (c) C1-3, ε=1.6, t=1000 s

Acknowledgments

This research work has been supported by the KMB project (193179/I40) in Norway. The financial support by the Research Council of Norway and the industrial partners, Hydro Aluminium and Sapa Technology is gratefully acknowledged. Ke HUANG acknowledges the financial support from NTNU, through the Strategic Area Materials.

References

[1] HUMPHREYS F J. The nucleation of recrystallization at second phase particles in deformed aluminium [J]. Acta Metallurgica, 1977, 25(11): 1323−1344.

[2] DOHERTY R D, HUGHES D A, HUMPHREYS F J, JONAS J J, JUUL JENSEN D, KASSNER M E, KING W E, MCNELLEY T R, McQUEEN H J, ROLLETT A D. Current issues in recrystallization: A review [J]. Materials Science and Engineering A, 1997, 238(2): 219−274.

[3] HUMPHREYS F J. A unified theory of recovery, recrystallization and grain growth, based on the stability and growth of cellular microstructures-I. The basic model [J]. Acta Materialia, 1997, 45(10): 4231−4240.

[4] HUMPHREYS F J. Particle stimulated nucleation of recrystallization at silica particles in nickel [J]. Scripta Materialia, 2000, 43(7): 591−596.

[5] DAALAND O, NES E. Recrystallization texture development in commercial Al−Mn−Mg alloys [J]. Acta Materialia, 1996, 44(4): 1413−1435.

[6] ZHANGY H, JUUL JENSEN D, ZHANG Y B, LIN F X, ZHANG Z Q, LIU Q. Three-dimensional investigation of recrystallization nucleation in a particle-containing Al alloy [J]. Scripta Materialia, 2012, 67(4): 320−323.

[7] NES E, RYUM N, HUNDERI O. On the Zener drag [J]. Acta Metallurgica, 1985, 33(4): 11−22.

[8] HUMPHREYS F J, HATHERLY M. Recrystallization and related annealing phenomena [M]. 2nd ed. Oxford, United Kingdom: Elsevier Science Ltd, 2004.

[9] HUMPHREYS F J, KALU P N. Dislocation-particle interactions during high temperature deformation of two-phase aluminium alloys [J]. Acta Metallurgica, 1987, 35(12): 2815−2829.

[10] HUTCHINSON W B, OSCARSSON A, KARLSSON Å. Control of microstructure and earing behaviour in aluminium alloy AA 3004 hot bands [J]. Materials Science and Technology, 1989, 5(11): 1118−1127.

[11] OSMAN M, ENGLER O, KARHAUSEN K, LÖCHTE L, MCLAREN A J. Effect of homogenisation conditions on recrystallisation in Al−Mg−Mn alloy AA 5454 [J]. Materials Science and Technology, 2007, 23(6): 688−698.

[12] ENGLER O, LIU Z, KUKNKE K. Impact of homogenization on particles in the Al−Mg−Mn alloy AA 5454 — Experiment and simulation [J]. Journal of Alloys and Compounds, 2013, 560(25): 111−122.

[13] ENGLER O, LAPTYEVA G, WANG N. Impact of homogenization on microchemistry and recrystallization of the Al−Fe−Mn alloy AA 8006 [J]. Materials Characterization, 2013, 79: 60−75.

[14] BIROL Y. Impact of homogenization on recrystallization of a supersaturated Al−Mn alloy [J]. Scripta Materialia, 2009, 60(1): 5−8.

[15] BIROL Y. Optimization of homogenization for a low alloyed AlMgSi alloy [J]. Materials Characterization, 2013, 80: 69−75.

[16] TOTIK Y, GAVGALI M. The effect of homogenization treatment on the hot workability between the surface and the center of AA 2014 ingots [J]. Materials Characterization, 2002, 49: 261−268.

[17] RADETIC T, POPOVIC M, ROMHANJI E. Microstructure evolution of a modified AA5083 aluminum alloy during a multistage homogenization treatment [J]. Materials Characterization, 2012, 65: 16−27.

[18] DU Q, POOLE W J, WELLS M A, PARSON N C. Microstructure evolution during homogenization of Al−Mn−Fe−Si alloys: Modeling and experimental results [J]. Acta Materialia, 2013, 61(13): 4961−4973.
[19] HUANG K, WANG N, LI Y J, MARTHINSEN K. The influence of microchemistry on the softening behavior of cold-rolled Al−Mn−Fe−Si alloys [J]. Materials Science and Engineering A, 2014, 601: 86−96.
[20] HUANG K, LI Y J, MARTHINSEN K. Isothermal and non-isothermal annealing of cold-rolled Al−Mn−Fe−Si alloy with different microchemistry states [J]. Materials Science Forum, 2014, 783−786: 174−179.
[21] HUANG K, LI Y J, MARTHINSEN K. Microstructural evolution during isothermal annealing of a cold-rolled Al−Mn−Fe−Si alloy with different microchemistry states [J]. Materials Science Forum, 2014, 794−796: 1163−1168.
[22] WANG N, FLATØY J E, LI Y J, MARTHINSEN K. Evolution in microstructure and mechanical properties during back-annealing of AlMnFeSi alloy [J]. Transactions of Nonferrous Metals Society of China, 2012, 22: 1878−1883.
[23] WANG N, LI Y J, MARTHINSEN K. Characterization the softening behavior of cold rolled AlMnFeSi-alloys during conditions of concurrent precipitation [J]. Materials Science Forum, 2013, 753: 231−234.
[24] MUGGERUD A M F, MØRTSELL E A, LI Y J, HOLMESTAD R. Dispersoid strengthening in AA3xxx alloys with varying Mn and Si content during annealing at low temperatures [J]. Materials Science and Engineering A, 2013, 567(1): 21−28.
[25] HERSENT E, HUANG K, FRIIS J, MARTHINSEN K. Modelling the evolution in microchemistry and its effects on the softening behavior of cold rolled AlFeMnSi-alloys during annealing [J]. Materials Science Forum, 2013, 753: 143−146.
[26] MARTHINSEN K, WANG N, HUANG K. Modelling microstructure and properties during annealing of cold-rolled Al−Mn−Fe−Si-alloys with different microchemistries [J]. Materials Science Forum, 2014, 783−786: 57−62.
[27] LI Y J, ARNBERG L. Evolution of eutectic intermetallic particles in DC-cast AA3003 alloy during heating and homogenization [J]. Materials Science and Engineering A, 2003, 347(1−2): 130−135.
[28] ENGLER O, RANDLE V. Introduction to texture analysis: Macrotexture, microtexture and orientation mapping [M]. 2nd ed. Bota Raton FL: CRC Press, 2010.
[29] TANGEN S, SJØLSTAD K, FURU T, NES E. Effect of concurrent precipitation on recrystallization and evolution of the P-texture component in a commercial Al−Mn alloy [J]. Metallurgical and Materials Transactions A, 2010, 41(11): 2970−2983
[30] SOMERDAY M, HUMPHREYS F J. Recrystallization behavior of supersaturated Al−Mn alloys, Part 1, Al−1.3wt%Mn [J]. Materials Science and Technology, 2003, 19: 20−29.

冷轧不同微量化学状态 Al−Mn−Fe−Si 铝合金的等温退火

黄 科[1]，李彦军[1,2]，Knut MARTHINSEN[1]

1. Department of Materials Science and Engineering, Norwegian University of Science and Technology (NTNU), Trondheim 7491, Norway;
2. SINTEF Materials and Chemistry, Trondheim 7465, Norway

摘 要：通过 3 种不同热处理工艺使一种 Al−Mn−Fe−Si 合金获得了不同固溶液和不同尺寸及数量的弥散析出相，包括铸造态，一种富含高密度、细小、弥散相的状态，另外一种状态则仅有少量、相对粗大的弥散相。采用 EBSD 技术系统研究冷轧后退火过程中微观组织的演变以及初始组织状态对再结晶动力学、再结晶晶粒形貌和织构的影响。结果表明，再结晶动力学、最终微观组织和织构由加工条件和合金的初始组织和固溶度决定。高密度弥散析出相阻止形核，显著阻碍软化过程，最终得到粗大的狭长晶粒以及 P 和 ND-rotated cube 织构。在没有预先存在的细小、稠密的弥散相并且在退火过程中弥散相析出数量很少的时候则能更快完成再结晶并得到均匀、细小的等轴晶以及显著的立方织构。

关键词：铝合金；Al−Mn−Fe−Si 合金；再结晶动力学；微量化学；析出相；再结晶织构

(Edited by Xiang-qun LI)